International Journal of Engineering

Fracture Mechanism of CoCrMo Porous Nano-composite Prepared by Powder Metallurgy Route

M. Taghian Dehaghani*, M. Ahmadian

Department of Materials Engineering, Isfahan University of Technology, Isfahan, Iran

A B S T R A C T

The main aim of this research was to find the mechanism for the failure of the CoCrMo porous nano-composite by characterizing microstructural changes and fractured surface after compression test. For this purpose, porous nano-composites were prepared with the addition of bioactive glass nano-powder to Co-base alloy with 22.5% porosity by the combination of space-holder and powder metallurgy techniques. The micrographs of samples showed that porous nano-composites had the micro and macro pores including open and closed pores. The observed fracture surface in the triple conjunction of sintered powders indicated a complex of intergranular and transgranular fracture mechanisms. The brittle carbide phase related to the higher solute content (Cr and Mo) precipitated at grain boundaries, leading to the intergranular fracture mechanism and transgranular mechanism that was due to the phase transformation during compression test.

doi: 10.5829/ije.2018.31.01a.03

1. INTRODUCTION

Porous metals with a combination of metals and porous materials properties have emerged as a new class of materials. These materials exhibit unusual mechanical and thermal properties, including energy absorption, vibrational and acoustic damping, and thermal insulation which lead to a wide range of applications in heat exchanger, blast resistance, catalyst and so on [1-3]. The porous metals productions are grouped into four methods: (i) aqueous solutions of metal powder by baking and sintering, (ii) liquid metallurgy, (iii) gas injection in liquid metals, and (iv) solid state method through powder metallurgy techniques [4-6]. Powder-metallurgical (P/M) techniques enable the production of base metal parts with finer grain structures and so enhanced properties, especially strength, toughness and ductility [7, 8]. Space-holder technique (a powder metallurgy method) which is a production process that can produce porous metal of greater porosity was first employed by Zhao and Sun for producing porous aluminum [9]. In this technique, the spacer particles

make the space within the structure and therefore allow accurate and simple control of pore morphology, fraction and interconnectivity in the structure.

Cobalt and its alloys are widely used because of its excellent corrosion and wear resistance and biocompatibility. However, two main problems with this alloy are the high elastic modulus and non-bioactivity. In this respect, many attempts have been made by researchers through applying heat treatment and introducing porosity and bioactive materials to improve the biological and mechanical properties of this alloy [10-13].

One of the most appropriate bioactive materials is 58S bioglass (58S: 58% SiO_2-38% CaO-4% P_2O_5, all in mol%). This material which can be synthesized by sol–gel method, as shown by the TEM image in Figure 1, has quasi-spherical morphology with a mean diameter of about 90 nm [14].

Briefly, the aim of present study was to characterize the microstructural and mechanical properties of CoCrMo porous nano-composite and to find fracture mechanism during compression test.

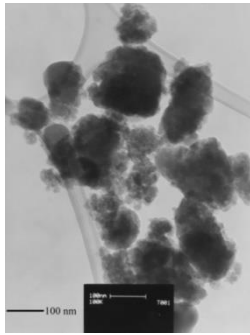*Corresponding Author's Email: majid.taghian@yahoo.com* (M. Taghian Dehaghani)

Figure 1. TEM image of 58S bioglass nano-particles

2. MATERIALS AND METHODS

2. 1. Raw Materials   Gas atomized Co-base powder (Co-28 wt% Cr-5.3 wt% Mo) with about 130 μm in diameter according to the ISO standard 58342-4 (E) (ISO-1996) was supplied by Carpenter Co. (Sweden). As can be seen in Figure 2, these alloy powder particles have a spherical shape with about 130 μm in diameter.

NH_4HCO_3 (ammonium hydrogen carbonate) with nearly cubic shapes and PVA (polyvinyl alcohol) solution (5 wt% PVA + 95 wt% water) have been used as space-holder and organic binder, respectively. Space-holder particles purchased from Uni-Chem were sieved using standard ASTM sieves to the range of 250–500 μm.

2. 2. Sample Preparation   The flowchart of the process to prepare specimens in this study is given in Figure 3. The sample preparation process consists of mixing, compacting, removing space-holder and sintering stages. In this way, The Co-base alloy powder, fifteen weight percent of bioglass nano-powder, NH_4HCO_3 and two weight percent of PVA solution were mixed together for 15 min in a shaker-mixer to ensure the homogeneous distribution of the components. The obtained powder mixture was cold compacted in a cylindrical die of 5 mm diameter with a pressure of around 200 MPa and crosshead speed of 5 mm/min.
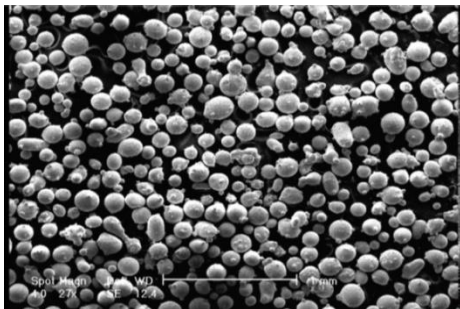

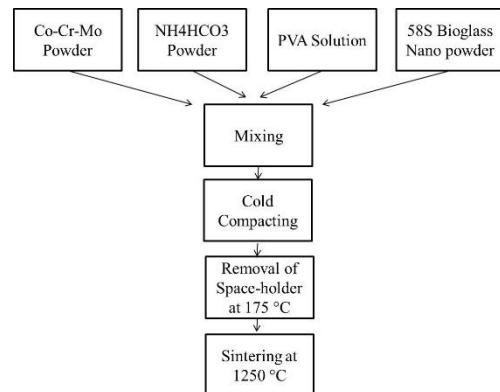**Figure 2.** SEM micrograph of gas-atomized Co–Cr–Mo alloy powder

Figure 3. Flowchart of the process employed to prepare CoCrMo Porous Nano-composite specimens

The space-holder removal and sintering stages were done at 175°C and 1250°C, respectively each for 2 h under high-purity argon gas.

2. 3. Characterization   Compressive tests were done by a universal testing machine (UTM) (Universal Hounsfield, H25ks, England) according to ASTM E9-09.

Scanning electron microscope (SEM, Philips XL 30) and optical microscope (OM, Nikon, Epiphot, Japan) were used in order to investigate pores and microstructural features of the samples. In addition, in order to investigate the failure mode and fracture patterns after compression tests, the fractured surfaces were subjected to SEM analysis. For observation of the changes in the microstructure arisen in the samples during sintering process, samples before and after sintering were mounted in epoxy resin and were then ground and polished to a mirror-like surface. Finally, samples were etched with 6:1 HCl to H_2O_2 solution and investigated by optical microscope.

The phase analysis of the as-received metal powder and sintered samples before and after compression test was characterized by means of a Philips X'pert-MPD X-ray diffraction instrument with Cu k_α radiation in the range of 30°<2θ< 100° ($\lambda_{Cu\ K\alpha}$= 0.154186 nm, radiation at 30 mA and 40 kV).

3. RESULTS AND DISCUSSION

SEM micrograph of sample containing 22.5% porosity is shown in Figure 4. Also, Figure 5a and b show OM micrographs of polished cross-section of the Co-base alloy powder in the as-received condition and the sample sintered at 1250°C for 2 h after etching treatment, respectively. From Figure 4, it is evident that even after sintering process powder particles retained their original shapes, leading to the interstitial sites around particles in the sample.
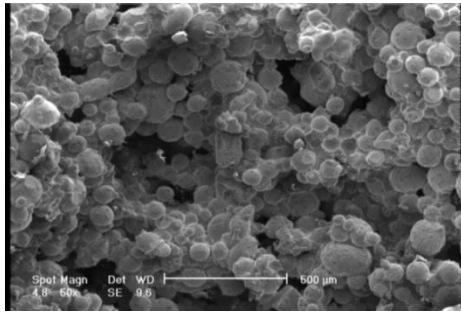
Figure 4. SEM micrograph of sample with 22.5% porosity

Indeed, due to spherical nature and smooth surface of Co-base alloy particles, relatively less extent of connectivity among the powder particles is expected. Thus, under the present condition of sintering, there is a possibility of having reasonably large amount of micro-pores due to the interstitial locations around Co-base alloy particles in the samples even after sintering. Remaining spherical shapes of powder particles as a result of partial sintering can lead to the rough inner surface of pores and sharp radius of curvature, as shown in Figure 5b. As will be discussed later, sharp radius of curvatures results in the high stress concentration areas, fracture in neck between the particles during compression test. In addition to micro-pores there is also other type of pores with sizes larger than about 250 μm. These pores, called macro-pores, are due to the decomposition of ammonium hydrogen carbonate particles in the first stage of heat treatment. In other words, the elongated shapes of macro-pores distributed uniformly replicate the initial shape of the ammonium hydrogen carbonate particles.

In agreement with previous reports, as can be seen in Figure 5a, the alloy in the as-cast condition presents a microstructure consisting of irregular, dendritic metastable matrix (γ phase) and precipitates composed mainly of the $M_{23}C_6$ carbide (M=Cr, Mo and Co) "eutectic" with blocky morphology which appear in interdendritic regions and grain boundaries [15, 16]. This metastable structure refinement with random dendritic directions is caused by rapid solidification from the liquid state. However, as it is clear from Figure 5b, the dendritic structure changes its morphology from a directional dendritic structure to a homogeneous equiaxial grain structure. Furthermore, the morphology of carbide phase changed from blocky shape into globular that exists non-continuously at the grain boundaries. This brittle phase related to the higher solute content (Cr, Mo) at grain boundaries causes a stress concentration, leading to the fracture during compression test.

Figure 6a indicates X-ray diffraction pattern of Co-base alloy in the as-received condition.
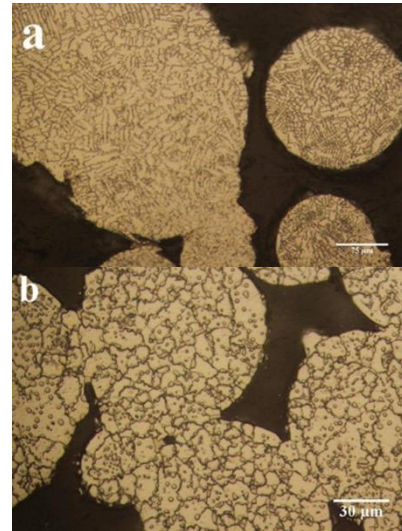

Figure 5. Optical micrographs of (a) the Co-base alloy powder in the as-received condition, showing dendrite microstructure and (b) the sample sintered at 1250 °C for 2 h, showing Precipitation of carbides at the grains boundaries.

It is evident from this pattern that there are strong peaks related to the FCC phase (PDF # 15-0806, Fm-3m,c), only. The pattern shown in Figure 6b is related to the sample sintered at 1250°C for 2 h. The comparison of these patterns demonstrates that except for 58S bioglass peaks there is no new phase formation detectable on the sintered sample. Furthermore, a shift of the diffraction peaks to lower values of 2θ is observed, which is reflected in an increase in the lattice parameter. As will be discussed later, this fact could be related to the microstructural change which occurred during sintering process. It is worth mentioning that pure cobalt undergoes an allotropic transformation from the hexagonal close-packed structure (HCP, ε-phase) to a face centered cubic structure (FCC, γ-phase) above 417°C [17-20]. Some elements such as Cr and Mo stabilize γ phase and increase this transformation temperature (T_C). For instance, T_C is increased toward about 970°C in Co-27Cr-5Mo-0.05C wrought alloys [21]. As the γ phase has more slip systems compared to the ε phase, in this respect achievement of γ phase is important. Therefore, the crystal structure in the matrix phase is controlled to be the γ phase to attain higher ductility.

As mentioned before, in the XRD pattern presented in Figure 6b, a shift of the diffraction peaks to lower values of 2θ is observed which shows an increase in the lattice parameter. According to the popular hard-sphere assumption, the atomic radius f Co in the pure state is R_{Co} = 1.67 Å while that of Cr in the pure state is R = 1.25 Å. This suggests that if the Cr precipitates from the Co matrix, the Co matrix lattice parameter will be increased.
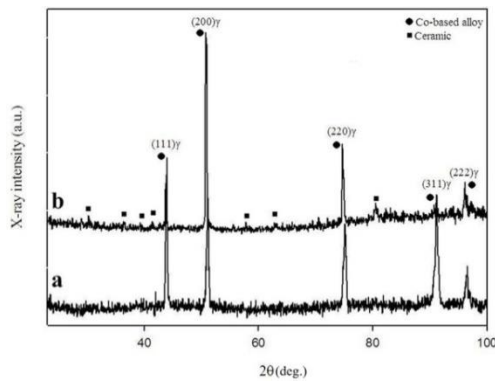
Figure 6. X-ray diffraction patterns of (a) the Co-base alloy in the as-received condition and (b) the sample sintered at 1250 °C for 2 h

Figures 7a and b show digital camera images of the samples before and after compression test. Visual examination of the samples before compression test displays a good integrity for compression test. As can be seen in Figure 7b, the sample shows cracking along the plane angle of 45 degree with respect to the axis of the applied load that has maximum shear stress after compression test.

In order to determine the mechanism for the failure of the present samples after compression test, the fractured surfaces were subjected to SEM analysis. Figure 8a shows micrograph of the fracture surfaces in the triple conjunction. The observed fracture surfaces in the triple conjunction may be attributed to the aforementioned specific orientation and arrangement of the powder particles in the green samples and after sintering. At the primary stage of sintering, the geometric order of the particles, and their specific shape as determined by local radius of curvatures among particles, restrict the rate of sintering and necking phenomenon between the particles, which in turn specify the characteristics of the sintered samples [22, 23]. Generally, particles with a large radius of curvature do not provide a driving force for necking during sintering process as high as those of particles with a smaller radius of curvature.
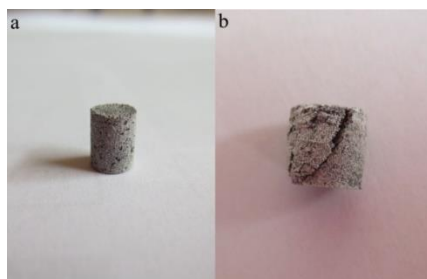

Figure 7. Digital camera image of the samples (a) before and (b) after compression test

The degree of sintering will be higher for smaller radius of curvature contacts resulting from higher atom transfer [22]. It is well known that cracks are originated in high-stress sites (stress concentration regions) [24]. The presence of pores and the geometry of sinter neck regions within the samples provide stress concentration sites where crack initiation readily occurs. Subsequently, the cracks will propagate along paths with the least resistance to crack progress. In addition, according to SEM photographs observed in Figures 8b and c, there are two distinct fracture mechanisms in neck region that leads to the crack propagation and separation between sintered particles. Based on the optical micrograph shown in Figure 5b, the grain boundaries are found to contain large globular carbides which promotes a rapid crack propagation path along the grain boundaries. The EDS spectra of the globular particles on the fractured bonded surface and SEM micrograph shown in Figure 8b confirms induced fracture along the grain boundaries. Indeed, propagating the cracks through these grain boundary carbides results in intergranular fracture. Figure 8c shows another one of surface fracture morphology. This micrograph indicates that transgranular cleavage fracture is formed from the initial intergranular mode in the surrounding neck region. But, cleavage facets form in body-centered cubic (BCC) and HCP metals when the crack path follows a well-defined transgranular crystallographic plane [25] that seems to be in contrast with FCC structure indicated by XRD pattern in Figure 6b. To clarify this ambiguity, the X-ray diffraction pattern was taken from fractured surface as shown in Figure 9. From this pattern it is observed that in addition to sharp peaks corresponding to the FCC phase there are also some peaks related to the HCP phase (PDF # 05-0727, P63/mmc, ε). This means that FCC→HCP phase transformation takes place during compression test leading to the cleavage fracture mechanism. Previous investigations show that the FCC phase is predominant at room temperature, but the FCC→HCP phase transformation could be isothermally or strain- induced [26-29]. For instance, Taghian et al. [28] have shown that strain-induced FCC→HCP phase transformation occurs during milling of Co-base alloy powder. In another work Balagna et al. [29] have shown that the HCP phase was induced during the wear tests through a strain induced mechanism of phase transformation, due to the applied load.

At the end, it is important to mention that the main goal of the use of 58S bioglass was the bioactivity property giving to the bio-inert Co-base alloy. However the effect of these particles on the grain growth during the sintering process and mechanical properties should be investigated in future.
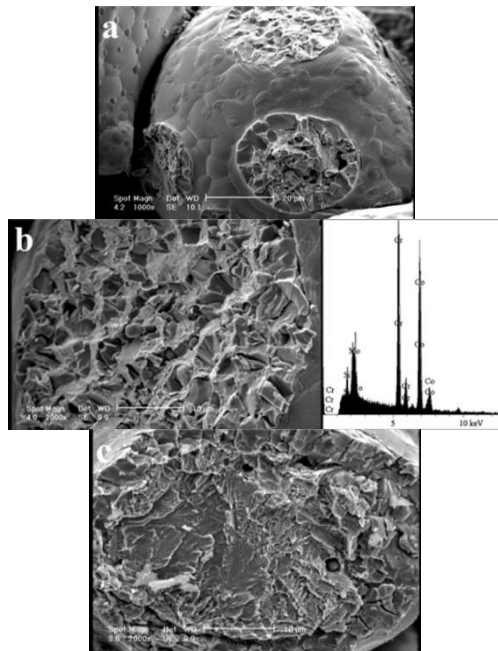
Figure 8. SEM micrographs of (a) the fracture surfaces in the triple conjunction produced by (b) intergranular fracture due to carbides particles and (c) transgranular fracture cleavage mechanism
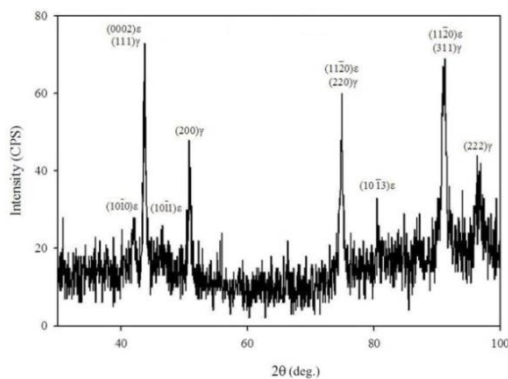

Figure 9. X-ray diffraction pattern of the fracture surface

4. CONCLUSIONS

Co-base porous nano-composites having 22.5% porosity were fabricated using space-holder and powder metallurgy techniques. Fabricated porous nano-composites have the micro and macro pores including open and closed pores. Microstructure changes after sintering process indicate that the dendritic structure changes its morphology from a directional dendritic structure to a homogeneous equiaxial grain structure with globular carbide phase at the grain boundaries. This brittle phase related to the higher solute content (Cr, Mo) at grain boundaries causes a stress concentration, leading to the fracture during compression test. The observed fracture surfaces in the triple conjunction of sintered powders caused by partial sintering and large radius of curvature among particles, show a complex of intergranular and transgranular fracture mechanisms. These fracture mechanisms are due to the carbide precipitates concentrated at grain boundaries during sintering process and FCC→HCP phase transformation during compression test.

5. REFERENCES

1.   Davies, G. and Zhen, S., "Metallic foams: Their production, properties and applications", *Journal of Materials Science*, Vol. 18, No. 7, (1983), 1899-1911.

2.   Lu, T. and Chen, C., "Thermal transport and fire retardance properties of cellular aluminium alloys", *Acta Materialia*, Vol. 47, No. 5, (1999), 1469-1485.

3.   Ebadzadeh, T., "Infiltration of porous zircon preforms with alumina precursor", *International Journal Of Engineering-Materials And Energy Research Center-*, Vol. 18, No. 3, (2005), 295.

4.   Baumgärtner, F., Duarte, I. and Banhart, J., "Industrialisation of p/m foaming process", *Advanced Engineering Materials*, Vol. 2, No. 4, (2000), 168-174.

5.   Stanzick, H., Wichmann, M., Weise, J., Helfen, L., Baumbach, T. and Banhart, J., "Process control in aluminum foam production using real-time x-ray radioscopy", *Advanced Engineering Materials*, Vol. 4, No. 10, (2002), 814-823.

6.   Gergely, V. and Clyne, B., "The formgrip process: Foaming of reinforced metals by gas release in precursors", *Advanced Engineering Materials*, Vol. 2, No. 4, (2000), 175-178.

7.   Patel, B., Inam, F., Reece, M., Edirisinghe, M., Bonfield, W., Huang, J. and Angadji, A., "A novel route for processing cobalt–chromium–molybdenum orthopaedic alloys", *Journal of The Royal Society Interface*, (2010), rsif20100036.

8.   Dewidar, M.M., Yoon, H.-C. and Lim, J.K., "Mechanical properties of metals for biomedical applications using powder metallurgy process: A review", *Metals and Materials International*, Vol. 12, No. 3, (2006), 193-200.

9.   Zhao, Y. and Sun, D., "A novel sintering-dissolution process for manufacturing al foams", *Scripta materialia*, Vol. 44, No. 1, (2001), 105-110.

10. Wojnar, L., Dąbrowski, J.R. and Oksiuta, Z., "Porosity structure and mechanical properties of vitalium-type alloy for implants", *Materials Characterization*, Vol. 46, No. 2, (2001), 221-225.

11. Dehaghani, M.T. and Ahmadian, M., "Effect of sintering temperature and time on the mechanical properties of Co–Cr–Mo/58s bioglass porous nano-composite", *Bulletin of Materials Science*, Vol. 38, No. 5, (2015), 1239-1246.

12. Oksiuta, Z., Dabrowski, J. and Olszyna, A., "Co–cr–mo-based composite reinforced with bioactive glass", *Journal of Materials Processing Technology*, Vol. 209, No. 2, (2009), 978-985.

13. Giacchi, J., Morando, C., Fornaro, O. and Palacio, H., "Microstructural characterization of as-cast biocompatible Co–Cr–Mo alloys", *Materials Characterization*, Vol. 62, No. 1, (2011), 53-61.

14. Taghian Dehaghani, M., Ahmadian, M. and Fathi, M., "Synthesis, characterization, and bioactivity evaluation of amorphous and crystallized 58s bioglass nanopowders", *International Journal of Applied Ceramic Technology*, Vol. 12, No. 4, (2015), 867-874.

15. Atamert, S. and Bhadeshia, H., "Comparison of the microstructures and abrasive wear properties of stellite hardfacing alloys deposited by arc welding and laser cladding", *Metallurgical Transactions A*, Vol. 20, No. 6, (1989), 1037-1054.

16. Ozols, A., Sirkin, H. and Vicente, E., "Segregation in stellite powders produced by the plasma rotating electrode process", *Materials Science and Engineering: A*, Vol. 262, No. 1, (1999), 64-69.

17. Adams, R. and Altstetter, C., "Thermodynamics of the cobalt transformation", *Trans Met Soc Aime*, Vol. 242, No. 1, (1968).

18. Lopez, H. and Saldivar-Garcia, A., "Martensitic transformation in a cast co-cr-mo-c alloy", *Metallurgical and Materials Transactions A*, Vol. 39, No. 1, (2008), 8-18.

19. Huang, P. and Lopez, H., "Strain induced ε-martensite in a co–cr–mo alloy: Grain size effects", *Materials Letters*, Vol. 39, No. 4, (1999), 244-248.

20. Remy, L. and Pineau, A., "Twinning and strain-induced fcc→hcp transformation on the mechanical properties of c Co-Ni-Cr-Mo alloys", *Materials Science and Engineering*, Vol. 26, No. 1, (1976), 123-132.

21. Saldívar, A. and Lopez, H., "Role of aging on the martensitic transformation in a cast cobalt alloy", *Scripta materialia*, Vol. 45, No. 4, (2001), 427-433.

22. German, R.M., "Sintering theory and practice", *Solar-Terrestrial Physics (Solnechno-zemnaya fizika)*, (1996), 568.

23. Bannister, M., "Shape sensitivity of initial sintering equations", *Journal of the American Ceramic Society*, Vol. 51, No. 10, (1968), 548-553.

24. Green, D.J., "An introduction to the mechanical properties of ceramics, Cambridge University Press, (1998).

25. Becker, W. and Lampman, S., "Fracture appearance and mechanisms of deformation and fracture", *Materials Park, OH: ASM International, 2002.*, (2002), 559-586.

26. Chiba, A., Kumagai, K., Nomura, N. and Miyakawa, S., "Pin-on-disk wear behavior in a like-on-like configuration in a biological environment of high carbon cast and low carbon forged Co–29Cr–6Mo alloys", *Acta Materialia*, Vol. 55, No. 4, (2007), 1309-1318.

27. García, A.d.J.S.v., Medrano, A.M. and Rodríguez, A.S., "Effect of solution treatments on the fcc/hcp isothermal martensitic transformation in Co-27Cr-5Mo-0.05 c aged at 800 c", *Scripta Materialia*, Vol. 40, No. 6, (1999), 717-722.

28. Dehaghani, M.T., Ahmadian, M. and Fathi, M., "Effect of ball milling on the physical and mechanical properties of the nanostructured Co–Cr–Mo powders", *Advanced Powder Technology*, Vol. 25, No. 6, (2014), 1793-1799.

29. Balagna, C., Spriano, S. and Faga, M., "Characterization of co–cr–mo alloys after a thermal treatment for high wear resistance", *Materials Science and Engineering: C*, Vol. 32, No. 7, (2012), 1868-1877.

Fracture Mechanism of CoCrMo Porous Nano-composite Prepared by Powder Metallurgy Route

M. Taghian Dehaghani, M. Ahmadian

Department of Materials Engineering, Isfahan University of Technology, Isfahan, Iran

چکیده

هدف اصلی از این تحقیق یافتن سازوکار (مکانیزم) شکست نانوکامپوزیت متخلخل CoCrMo با مشخصه‌یابی تغییرات ساختاری و سطح شکسته شده بعد از آزمایش فشار بود. برای این منظور، نمونه‌های نانوکامپوزیت با تلفیقی از روش‌های متالورژی پودر و استفاده از مادهی فضاساز با افزودن نانوپودر شیشه زیست‌فعال به آلیاژ پایه کبالت و رسیدن به تخلخل ٪۲۲/۵ ساخته شد. تصاویر میکروسکوپی نمونه‌ها نشانگر وجود میکرو و ماکرو تخلخل‌ها، با ساختار باز و بسته بود. مشاهده سطح شکست در نواحی تف‌جوشی سه‌تایی پودری، ترکیبی از مکانیزم شکست بین‌دانه‌ای و داخل دانه‌ای را نشان می‌داد. رسوب فاز کاربیدی ترد نتیجهی انحلال مقادیر بالای عناصر محلول (کبالت و مولیبدن) منجر به مکانیزم شکست بین دانه‌ای و تحول فازی در حین کرنش در طول آزمایش فشار منجر به مکانیزم شکست داخل دانه‌ای شده بود.

doi: 10.5829/ije.2018.31.01a.03